APL Photonics

Ultra-compact and highly efficient silicon polarization splitter and rotator

Cite as: APL Photonics 1, 091304 (2016); https://doi.org/10.1063/1.4965832
Submitted: 26 July 2016 • Accepted: 09 October 2016 • Published Online: 18 November 2016

Yong Zhang, Yu He, Xinhong Jiang, et al.

Ultra-compact and highly efficient silicon polarization splitter and rotator

Yong Zhang,[1] Yu He,[1] Xinhong Jiang,[1] Boyu Liu,[1] Ciyuan Qiu,[1] Yikai Su,[1,a] and Richard A. Soref[2]
[1]*State Key Lab of Advanced Optical Communication Systems and Networks, Department of Electronic Engineering, Shanghai Jiao Tong University, Shanghai 200240, China*
[2]*Department of Engineering, The University of Massachusetts, Boston, Massachusetts 02125, USA*

(Received 26 July 2016; accepted 9 October 2016; published online 25 October 2016)

We propose and experimentally demonstrate an ultra-compact and highly efficient polarization splitter and rotator based on a silicon bent directional coupler structure. The TM-to-TE cross-polarization coupling occurs between the two parallel bent waveguides, if the phase matching condition is satisfied. Efficient polarization splitting and rotating are simultaneously achieved. The device is fabricated by a single step of exposure and etching. The measured peak TM-to-TE polarization conversion efficiency reaches 96.9%. The TM-to-TE conversion loss is lower than 1 dB in the wavelength range of 1544 nm–1585 nm, and the insertion loss for the TE polarization is lower than 0.3 dB in the wavelength regime of 1530 nm–1600 nm. The cross talk values are lower than −20 and −18 dB for the TE- and TM-polarizations over a wavelength range of 70 nm, respectively. The coupling length of the polarization splitter and rotator is 8.77 μm. To the best of our knowledge, our device achieves the shortest coupling length. [http://dx.doi.org/10.1063/1.4965832]

Silicon photonics on a silicon-on-insulator (SOI) platform has attracted much attention in the past decades[1,2] due to the advantages of compact footprint, low power consumption, and compatibility with the complementary metal-oxide-semiconductor (CMOS) process. The high index contrast property of silicon nano-waveguides allows for compact footprint and dense integration. However, it results in high polarization dependence for silicon photonic devices.[3] Generally, polarization-diversity schemes are applied to eliminate the polarization sensitivities.[4] The key elements for realizing the polarization-diversity are polarization beam splitters (PBSs)[5,6] and rotators (PSRs).[7,8] Many types of silicon-waveguide PBSs and PSRs have been reported based on various structures, including directional coupler,[9,10] multimode interference (MMI),[11] hybrid plasmonic waveguide,[12] grating,[13] photonic crystal,[14] and so on.

If two orthogonal modes have equal effective refractive indices and optical paths, and the vertical or horizontal symmetry is broken, cross-polarization coupling can occur. One polarization is therefore effectively converted to the other one. Previously, an efficient polarization convertor was realized based on the cross-polarization coupling effect[10] by breaking the vertical symmetry with air as the top-cladding material. The widths of the two parallel fully etched straight waveguides were carefully designed to satisfy the phase-matching condition. An insertion loss of <0.6 dB and cross talk value of −12 dB were achieved in the device with a coupling length of 36.8 μm. In order to realize a fabrication-error tolerant PSR, a tapered directional coupler was applied.[15] Similar high polarization conversion efficiencies were obtained in the device with a coupling length of 140 μm. A highly efficient silicon PSR with a double-etched waveguide was reported based on a double-etched direction coupler with a length of 27 μm.[16] The TM-to-TE conversion loss was lower than 0.5 dB, and the cross talk value

[a]Author to whom correspondence should be addressed. Electronic mail: yikaisu@sjtu.edu.cn.

was lower than −20 dB in the wavelength range of 30 nm. Recently, we fabricated an ultra-compact PSR based on a silicon bent directional coupler with a length of 8.77 μm and presented preliminary experimental results.[17] However, the cross talk values were <−10 dB, which should be reduced for practical applications.

In this paper, we perform a detailed study of the ultra-compact PSR in terms of device principle, optimization, and fabrication. The TM-to-TE cross-polarization coupling occurs between two parallel silicon bent waveguides. The widths of the bent waveguides are carefully designed and optimized to satisfy the phase-matching condition. The peak TM-to-TE polarization conversion efficiency reaches 96.9%. The TM-to-TE conversion loss is lower than 1 dB in the wavelength range of 1544 nm –1585 nm, and the insertion loss for the TE polarization is lower than 0.3 dB in the wavelength regime of 1530 nm–1600 nm. The cross talk values are lower than −20 and −18 dB for the TE- and TM-polarizations over a wavelength range of 70 nm, respectively, which are much better than our previous results.[17] The coupling length is 8.77 μm. To the best of our knowledge, our device achieves record short coupling length.

The 3D and top views of the structure of the proposed PSR device are plotted in Figs. 1(a) and 1(b), respectively. It consists of two parallel silicon bent waveguides (WG 1 and WG 2) coupled to each other. To achieve an efficient TM-TE cross-polarization conversion, a material which is different from the bottom silicon oxide layer should be applied as the top cladding layer. In the design, air is adopted as the top cladding. The widths of the two bent waveguides are optimized so that the fundamental TM mode in WG 1 and the fundamental TE mode in WG 2 have equal optical path lengths, i.e., the phase matching condition is satisfied. In this case, an efficient TM-TE cross-polarization coupling between the two bent waveguides occurs. The TM-polarized light in WG 1 is coupled to WG 2 and is simultaneously converted to the TE-polarized light. High efficiency TE-polarized light is obtained at the Cross port. On the other hand, due to the birefringence of the silicon nano-waveguides, the phase matching condition between the TE mode in WG 1 and any guided mode in WG 2 cannot be satisfied. Thus, the TE-polarized light passes through WG 1 without coupling and outputs at the Bar port.

The widths of the two parallel bent waveguides are optimized to satisfy the phase-matching condition, i.e., their optical path lengths (OPLs) are equal. Thus,

$$OPL = n_1 k_0 R_1 \theta = n_2 k_0 R_2 \theta, \tag{1}$$

$$n_1 R_1 = n_2 R_2, \tag{2}$$

where n_1 and n_2 are the effective indices of the fundamental TM mode and TE mode of WG 1 and WG 2, respectively, R_1 and R_2 are the corresponding bending radii, k_0 is the wave number in vacuum, and θ is the arc-angle for the coupling region.

The thickness of the top silicon layer of the SOI wafer is 220 nm. The effective indices of the two bent waveguides are calculated by the finite-difference time-domain (FDTD) method. The widths of the two bent waveguides, WG 1 and WG 2, are optimized to be w_1 = 588 nm and w_2 = 315 nm, respectively. In this case, the cross-polarization coupling between the two bent waveguides is achieved. Adiabatic tapers can be used for coupling to a conventional single-mode silicon waveguide at the input and output ports of the PSR. The bending radius of WG 1 is R_1 = 20 μm,

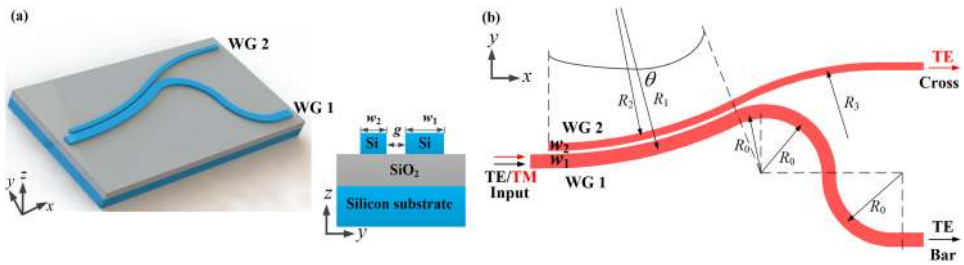

FIG. 1. The schematic configuration of the proposed silicon PSR based on a bent directional coupler, (a) the 3D view, (b) the top view.

which is a trade-off between achieving low bending losses for both polarizations and increasing the phase mismatching for the non-coupled polarization. The gap between the two bent waveguides is g = 140 nm, which is large enough to simplify the fabrication process. The bending radius of WG 2 is $R_2 = R_1 - (w_1 + w_2)/2 - g = 19.409$ μm. The coupling length is determined by the angle θ of the coupling region. θ is optimized such that the bent directional coupler operates in telecom C band. The angle θ is optimized to be 26°, and the corresponding coupling length is $L_c = R_1 \sin(\theta) = 8.77$ μm. The bends with a bending radius $R_0 = 3$ μm at the Bar port are designed to filter the undesired TM-polarized light and separate the two output waveguides. The bend at the Cross port has a radius of $R_3 = 14$ μm to guarantee a low bending loss.

The propagation of the optical field in the proposed PSR device is simulated by the three-dimensional FDTD method. The simulated power distributions at the plane of z = 0 for the TE- and TM-polarized light inputs are shown in Figs. 2(a) and 2(b), respectively. The wavelength is 1550 nm for the simulations. The four insets depict the mode distributions at the cross section of yz of input and output ports. Note that the simulated mode distribution at the cross section of yz of the Cross port for the TM-polarized input shows that the output is the fundamental TE mode supported by a waveguide of 315-nm width. The profile looks like a second order TE mode. We attribute it to the small width of the silicon waveguide (315 nm). When the TM-polarized light is injected into the Input port, the optical signal is coupled and simultaneously converted to the TE-polarized light, then outputs from the Cross port. While for the TE-polarized light input, the optical signal passes through the waveguide and outputs from the Bar port. The TM-polarized light is separated from the TE-polarized light and simultaneously rotated by the bent directional coupler.

In the experiment, a number of PSR devices were fabricated on a SOI wafer (220-nm-thick silicon on 3-μm-thick silica layer). First, E-beam lithography (EBL, Vistec EBPG 5200) was used to define the patterns of grating couplers on the ZEP520A resist. Then the patterns were transferred to the top silicon layer by inductively coupled plasma (ICP) dry etching using SF_6 and C_4F_8 gases with an etch depth of 70 nm. Second, the PSR structures were patterned on the wafer by EBL and ICP etching with a full etch depth of 220 nm. A scanning electron microscope (SEM) photo of a fabricated PSR based on a bent directional coupler is shown in Fig. 3(a). The magnified micrographs of the bent directional coupler are presented in Fig. 3(b).

To characterize the TM-TE coupling efficiency and cross talk performance of the PSR, four identical PSRs were fabricated to measure the transmission responses for the TE- and TM-polarized light inputs, respectively. The optical micrograph of the fabricated devices is shown in Fig. 3(d). In the measurements, grating couplers were used to couple the TE- and TM-polarized lights into/out

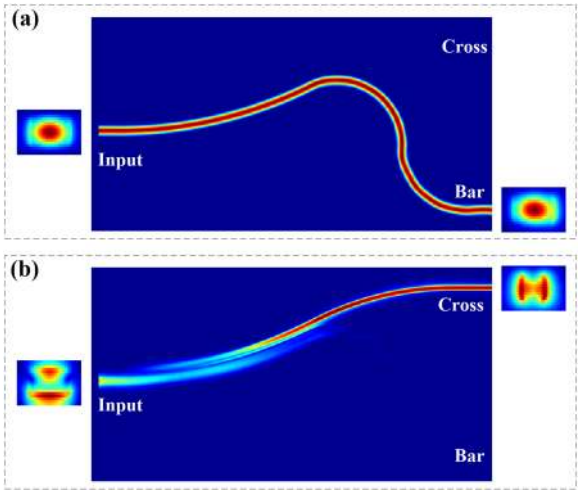

FIG. 2. (a) and (b) Simulated power distributions at the plane of z = 0 for the TE- and TM-polarized light inputs, respectively. The four insets depict the mode distributions at the cross section of yz of input and output ports.

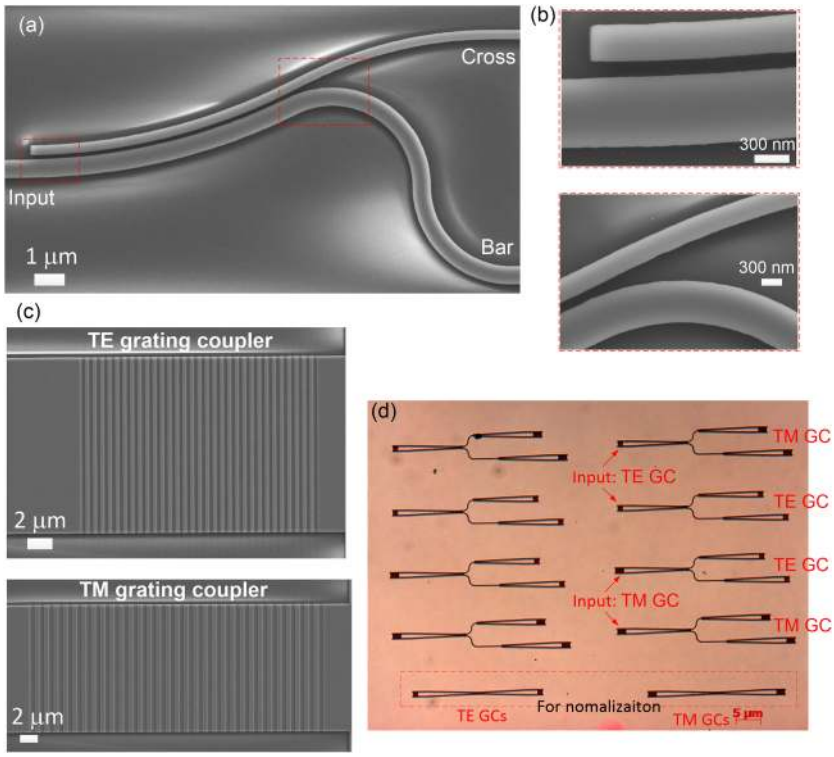

FIG. 3. (a) SEM photo of a fabricated PSR based on a bent directional coupler. (b) Magnified micrographs of the bent directional coupler. (c) SEM photos of fabricated TE- and TM-polarized grating couplers. (d) Optical micrograph of the fabricated devices.

of the chip. A tunable continuous wave (CW) laser (Keysight 81960A) was used to characterize the fabricated devices. The PSR transmission spectra can be obtained by scanning the laser wavelength and recording the output power. Both the TE and TM grating couplers were designed to achieve high polarization selectivity.[18] The period of the TE grating coupler is 630 nm and the filling factor is 48%. And those for the TM grating coupler are 1080 nm and 48%, respectively. The etching depth of both grating couplers is 70 nm. SEM photos of fabricated TE- and TM-polarized grating couplers are shown in Fig. 3(c). The coupling losses of the TE- and TM-polarized grating couplers are 5.6 dB/port and 7.0 dB/port at the central wavelengths of the gratings, respectively.

Figures 4(a) and (b) show the measured and simulated transmission responses at the cross and thru ports of the fabricated PSRs for the TE- and TM-polarized light inputs, respectively. The responses are normalized to the transmission of a straight waveguide with grating couplers. For the TE-polarized

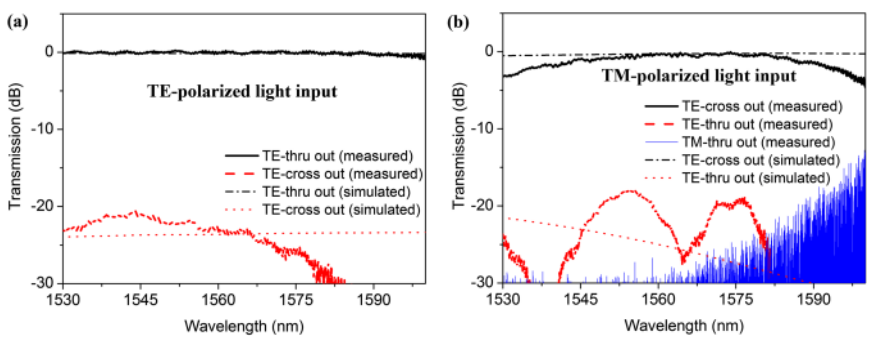

FIG. 4. Measured and simulated transmission responses at the cross and thru ports for the (a) TE-polarization and (b) TM-polarization. The thin dashed curves represent the simulated responses of the PSR by 3D-FDTD methods.

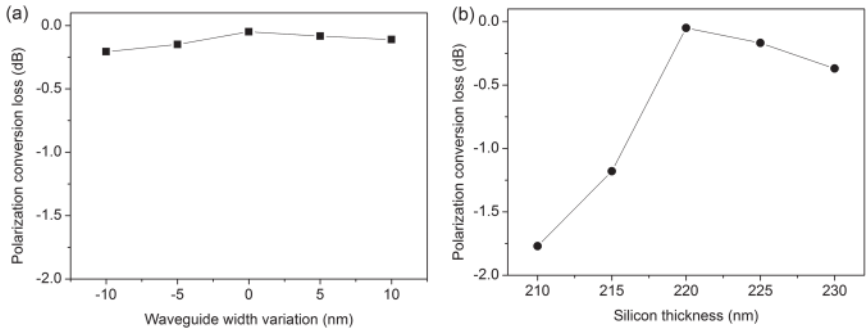

FIG. 5. Simulated polarization conversion losses of the devices with (a) different waveguide width variations and (b) different silicon thicknesses.

light input, high-efficiency TE-polarized light outputs from the Bar port, as shown in the solid black curve of Fig. 4(a). To obtain accurate peak conversion efficiency, we re-aligned the grating couplers, repeated the measurements several times, and took the average value. *The measurement errors in the transmission responses were less than 0.5 dB during multiple measurements*. The insertion loss is lower than 0.3 dB in the wavelength range of 1530 nm–1600 nm. The cross talk value for the TE-polarized light input is lower than −20 dB in the wavelength range of 1530 nm–1600 nm. For the TM-polarized light input, high-efficiency TE-polarized light output is obtained at the cross port, as depicted by the solid black curve of Fig. 4(b). We also measured the remaining TM-polarized light in the thru port, as depicted by the thin blue curve of Fig. 4(b). The noise at the longer wavelength is mainly due to the passband edges of the grating couplers that result in large fluctuation in the normalization process. The TM-to-TE coupling efficiency is a key parameter of the polarization rotator. The measured TM-to-TE coupling efficiency reaches its maximum of 96.9% at $\lambda = 1564$ nm, which corresponds to an insertion loss of 0.135 dB. In the wavelength range of 1544 nm–1585 nm, the TM-to-TE conversion loss is lower than 1 dB. The cross talk value for the TM-polarized light input is lower than −18 dB in the wavelength range of 1530 nm–1600 nm. The thin dashed curves in Fig. 4 represent the simulated responses of the PSR by 3D-FDTD methods. It is worth noting that the experimental results are in good agreement with the simulation results. The limited bandwidth is attributed to the bent directional coupler, which is restricted by the dispersion of the waveguide.

To investigate the fabrication tolerances, we study the polarization conversion losses with different waveguide width variations and silicon thicknesses by 3D-FDTD simulations and show the results in Figs. 5(a) and 5(b), respectively. The polarization conversion loss remains stable as the waveguide width varies. If the silicon thickness is higher than 220 nm, the polarization conversion loss does not

TABLE I. Comparison of various silicon polarization beam splitters and rotators.

Structures	Coupling length (μm)	Conversion loss (dB)	Cross talk (dB)	Bandwidth (nm)
Directional coupler[10]	36.8	0.6	<−12	C band
Tapered directional coupler[15]	140	0.5	-	C band
Double-etched directional coupler[16]	27	<0.5	<−20	30
Cascaded bi-level taper and DC[19]	475	<1.6	<−13	80
Cascaded taper and MMI[20]	190	0.6–2.5	<−12	100
Mode order conversions[21]	>53	<0.4	<−21	100
Rib directional coupler[a] [22]	24	>0.13	<−19	100
Taper-etched directional coupler[a] [23]	>80	0.09	<−30	160
Asymmetric coupler and MMI filter[24]	70	<1.5	<−20	50
Partially-etched 90° bends[a] [25]	10	>0.11	<−19	O band
Our work	8.77	0.135–1	<−18	41

[a]Simulation results.

experience significant degradation. Silicon photonics foundry of the Institute of Microelectronics, Singapore has reported that a 200-nm-wide fully etched waveguide yields 192 ± 4 nm width.[16] The data support that our proposal can be realized by the silicon photonics foundry.

Table I summarizes several reported results of the silicon PSRs and compares them with our device. It shows that our demonstrated PSR has the shortest coupling length, with low conversion loss and low cross talk value.

We have proposed and experimentally demonstrated an ultra-compact silicon PSR based on a bent directional coupler. The PSR utilizes the cross-polarization coupling effect between two parallel bent waveguides with air top-cladding, which is realized by a single etch process. The coupling length is as short as 8.77 μm. The measurement results show that the device can function as an efficient polarization splitter and rotator simultaneously. The peak TM-to-TE conversion efficiency reaches 96.9%. The TM-to-TE conversion loss is lower than 1 dB in the wavelength range of 1544 nm –1585 nm, and the insertion loss for the TE polarization is lower than 0.3 dB in the wavelength regime 1530 nm–1600 nm. The cross talk values are lower than −20 and −18 dB for the TE- and TM-polarizations over a wavelength range of 70 nm, respectively.

This work was supported in part by the National Natural Science Foundation of China (NSFC) under Grant No. 61235007/61505104, in part by the 863 High-Tech Program under Grant No. 2015AA017001, and in part by the Science and Technology Commission of Shanghai Municipality under Grant No. 15ZR1422800/16XD1401400. We thank the Center for Advanced Electronic Materials and Devices (AEMD) of Shanghai Jiao Tong University for the support in device fabrications.

[1] R. A. Soref, Silicon **2**, 1 (2010).
[2] V. R. Almeida, C. A. Barrios, R. R. Panepucci, and M. Lipson, Nature **431**, 1081 (2004).
[3] D. Dai, L. Liu, S. Gao, D. Xu, and S. He, Laser Photonics Rev. **7**, 303 (2013).
[4] P. Dong, X. Liu, S. Chandrasekhar, L. L. Buhl, R. Aroca, and Y. Chen, IEEE J. Sel. Top. Quantum Electron. **20**, 150 (2014).
[5] B. Shen, P. Wang, R. Polson, and R. Menon, Nat. Photonics **9**, 378 (2015).
[6] J. Chen, C. Sun, H. Li, and Q. Gong, Appl. Phys. Lett. **104**, 231111 (2014).
[7] A. Xie, L. Zhou, J. Chen, and X. Li, Opt. Express **23**, 3960 (2015).
[8] B. Troia, F. D. Leonardis, M. Lanzafame, T. Muciaccia, G. Grasso, G. Giannoccaro, C. E. Campanella, and V. Passaro, Adv. OptoElectron. **2014**, 1.
[9] L. Liu, Y. Ding, K. Yvind, and J. M. Hvam, Opt. Lett. **36**, 1059 (2011).
[10] L. Liu, Y. Ding, K. Yvind, and J. M. Hvam, Opt. Express **19**, 12646 (2011).
[11] B. Rahman, N. Somasiri, C. Themistos, and K. Grattan, Appl. Phys. B **73**, 613 (2001).
[12] X. Guan, H. Wu, Y. Shi, and D. Dai, Opt. Lett. **39**, 259 (2014).
[13] Y. Zhang, Y. He, J. Wu, X. Jiang, R. Liu, C. Qiu, X. Jiang, J. Yang, C. Tremblay, and Y. Su, Opt. Express **24**, 6586 (2016).
[14] X. Ao, L. Liu, L. Wosinski, and S. He, Appl. Phys. Lett. **89**, 171115 (2006).
[15] Y. Ding, L. Liu, C. Peucheret, and H. Ou, Opt. Express **20**, 20021 (2012).
[16] H. Guan, A. Novack, M. Streshinsky, R. Shi, Q. Fang, A. E. Lim, G. Lo, T. Baehr-Jones, and M. Hochberg, Opt. Express **22**, 2489 (2014).
[17] Y. Zhang, Y. He, X. Jiang, B. Liu, C. Qiu, and Y. Su, in The European Conference on Optical Communications (ECOC 2016), Düsseldorf, Germany, 18–22 September 2016.
[18] D. Taillaert, P. Bienstman, and R. Baets, Opt. Lett. **29**, 2749 (2004).
[19] W. D. Sacher, T. Barwicz, B. J. F. Taylor, and J. K. S. Poon, Opt. Express **22**, 3777 (2014).
[20] Y. Ding, H. Ou, and C. Peucheret, Opt. Lett. **38**, 1227 (2013).
[21] D. Chen, X. Xiao, L. Wang, W. Liu, Q. Yang, and S. Yu, Opt. Lett. **41**, 1070 (2016).
[22] J. Wang, B. Niu, Z. Sheng, A. Wu, X. Wang, S. Zou, M. Qi, and F. Gan, Opt. Express **22**, 4137 (2014).
[23] Y. Xiong, D. Xu, J. H. Schmid, P. Cheben, S. Janz, and W. N. Ye, Opt. Express **22**, 17458 (2014).
[24] D. Dai and H. Wu, in The Advanced Optical Congress 2016 (IPR, NOMA, Sensors, Networks, SPPCom, SOF), Vancouver, BC, Canada, 18–20 July 2016.
[25] K. Tan, Y. Hang, G. Lo, C. Lee, and C. Yu, Opt. Express **24**, 14506 (2016).